Magnetic properties of Co_NRh_M nanoparticles: experiment and theory†

M. Muñoz-Navia,‡[a] J. Dorantes-Dávila,[a] D. Zitoun,[b] C. Amiens,[b] B. Chaudret,[b] M.-J. Casanove,[c] P. Lecante,[c] N. Jaouen,[d] A. Rogalev,[d] M. Respaud[e] and G. M. Pastor*[f]

Received 4th April 2007, Accepted 9th May 2007
First published as an Advance Article on the web 28th September 2007
DOI: 10.1039/b705122k

The magnetism of Co–Rh nanoparticles is investigated experimentally and theoretically. The particles ($\approx$2 nm) have been synthesized by decomposition of organometallic precursors in mild conditions of pressure and temperature, under hydrogen atmosphere and in the presence of a polymer matrix. The magnetic properties are determined by SQUID, Mössbauer spectroscopy, and X-ray magnetic circular dichroism (XMCD). The structural and chemical properties are characterized by wide angle X-ray scattering, transmission electronic microscopy and X-ray absorption near edge spectroscopy. All the studied Co–Rh clusters are magnetic with an average spin moment per atom μ that is larger than the one of macroscopic crystals or alloys with similar concentrations. The experimental results and comparison with theory suggest that the most likely chemical arrangement is a Rh core, with a Co-rich outer shell showing significant Co–Rh mixing at the interface. Measured and calculated magnetic anisotropy energies (MAEs) are found to be higher than in pure Co clusters. Moreover, one observes that the MAEs can be tuned to some extent by varying the Rh concentration. These trends are well accounted for by theory, which in addition reveals important spin and orbital moments induced at the Rh atoms as well as significant orbital moments at the Co atoms. These play a central role in the interpretation of experimental data as a function of Co–Rh content. A more detailed analysis from a local perspective shows that the orbital and spin moments at the Co–Rh interface are largely responsible for the enhancement of the magnetic moments and magnetic anisotropy.

[a] *Instituto de Física, Universidad Autónoma de San Luis Potosí, Alvaro Obregón 64, San Luis Potosí, Mexico. E-mail: jdd@ifisica.uaslp.mx*
[b] *Laboratoire de Chemie de Coordination, CNRS, 205 route de Narbonne, 31077 Toulouse, France. E-mail: chaudret@lcc-toulouse.fr*
[c] *Centre d'Elaboration de Matériaux et d'Etudes Structurales, CNRS, 29 rue Jeanne Marvig, 31077 Toulouse, France. E-mail: casanove@cemes.fr*
[d] *European Synchroton Radiation Facility, 6 rue Jules Horowitz, BP220, 38043 Grenoble, France. E-mail: rogalev@esrf.fr*
[e] *Laboratoire de Physique et Chimie des Nano-objets, INSA, 135 avenue de Rangueil, 31077 Toulouse, France. E-mail: respaud@insa-toulouse.fr*
[f] *Institut für Theoretische Physik der Universität Kassel, Heinrich Plett Str. 40, D-34132 Kassel, Germany. E-mail: pastor@uni-kassel.de*

† The HTML version of this article has been enhanced with colour images.
‡ Present address: Max-Planck-Institut für Mikrostrukturphysik, D-06120 Halle, Germany. E-mail: mnavia@mpi-halle.mpg.de.

1. Introduction

The magnetism in monometallic ferromagnetic 3d transition-metal (TM) nanoparticles containing less than 1000 atoms has been the subject of numerous experimental and theoretical studies. It is nowadays relatively well understood that the large surface-to-volume ratio induces an enhancement of the spin and orbital magnetic moments and magnetic anisotropy energy (MAE) as compared to the bulk materials.[1,2] In contrast very little is known about the behaviour of magnetic nanoalloys. This subject is currently attracting considerable attention both from fundamental and technological perspectives. For example, for material science applications one would like to be able to develop magnetic nanoparticles that combine both high saturation magnetization (M_S) and large MAE. This can indeed be achieved by starting from a ferromagnetic (FM) 3d metal and by associating it with a second heavier element that displays a stronger spin–obit coupling and a potentially significant contribution to the total magnetization. Quite generally, 4d and 5d metals appear as very good candidates for this purpose. Co–Rh clusters are particularly appealing since Rh shows non-saturated magnetism in small clusters despite being non-magnetic in bulk.[3–7] Alloying Co with Rh should be an effective way to combine large magnetic moments with large magnetic anisotropy energy. In addition, the diversity of local chemical environments present in these nanoalloys and the competition between Co–Co, Co–Rh and Rh–Rh effective exchange couplings lead us to expect very interesting size and structural dependence of the magnetic properties.

In the past years some experimental and theoretical studies on Co–Rh nanoparticles have been performed. For instance, CoRh particles have been synthesized by Zitoun *et al.* by decomposing organometallic precursors in the presence of a polymer.[6] Moreover, the measurements have shown that the average magnetic moment per Co atom for clusters of about 300–400 atoms is about 2.38 μ_B for a Co concentration $x_{Co} \backsimeq 0.5$. This value is much larger than the average magnetization found in bulk alloys of similar concentration. From the point of view of theory only a few studies have been concerned with Co–Rh clusters. The interplay between structural, chemical and magnetic properties of small free Co_MRh_N ($N + m \leq 13$) have been determined by Dennler *et al.* within the framework of spin-density-functional theory.[7] They found that all studied Co–Rh clusters are magnetic with average and local spin moments that are often a factor two larger than those of macroscopic crystals or alloys with similar concentrations. It is the purpose of this paper to report on recent experimental and theoretical progress on the study of the magneto-anisotropic properties of Co_xRh_{1-x} clusters as a function of size, composition and structure.

2. Experimental

In the following we briefly review the experimental method to study the magnetic properties of Co–Rh clusters. Details of both the synthesis and the structural studies have been published in ref. 6 and 8. The nanoparticle synthesis is performed in solution by decomposition of organometallic precursors in the presence of a stabilizing polymer. These precursors decompose under hydrogen pressure (3 bars) at room temperature to give zero-valency atoms. The nucleation–growth process leads to the formation of metallic clusters. The use of organometallics allows us to work under mild conditions of temperature compared to thermal decomposition of a metal carbonyl compound ($Fe(CO)_5$ or $Co_2(CO)_8$). These methods lead to nanoparticle assemblies of well-defined size and composition. However, a passivated surface by carbon monoxide and/or carbides is highly probable. The decomposition of both organometallic precursors (Co and Rh) does not release any contaminating by-products in contrast to the reduction of a metal salt by a borohydride. Only cyclooctane and pentane-2,4-diol could bind to the nanocrystals surface. Surface

magnetism, which is crucial in small systems, is therefore not perturbed and the nanoparticle can be regarded as relatively close to the ideal free cluster from the magnetic point of view.

The organometallic approach combined with the use of polyvinylpyrrolidone K30 (PVP) at low metal concentration allows growth control of the nanoparticles. Three samples with Co final concentrations $x_{Co} = 0.76$, 0.49 and 0.25 were synthesized. The transmission electronic microscopy (TEM) studies evidence a regular dispersion of the clusters in the polymer matrix, with narrow log-normal size distributions, an average diameters around 2 nm, and a width below 15%. The analysis of the fine structure has been realized by using high resolution TEM and wide angle X-ray scattering (WAXS) techniques. The $Co_{0.25}Rh_{0.75}$ sample displays the bulk phase fcc structure with a first nearest neighbor (NN) distance of $d_{NN} \backsimeq 0.269$ nm. $Co_{0.49}Rh_{0.51}$ and $Co_{0.76}Rh_{0.24}$ do not display any conventional crystalline phase. The WAXS pattern can be fitted with a polytetrahedral structure,[9] and the interatomic distance evolves from $d_{NN} \backsimeq 0.269$ nm for $Co_{0.49}Rh_{0.51}$ to $d_{NN} \backsimeq 0.263$ nm for $Co_{0.76}Rh_{0.24}$ which confirms the bimetallic character of the nanoparticles. We may conclude that the clusters probably present a Rh core and a Co rich shell since d_{NN} is very close to that of bulk Rh. In conclusion, we may assume that the nanoparticles adopt a close packed crystalline structure with $d_{NN} \backsimeq d_{NN}$ (Rh).

Fig. 1 shows the hysteresis loops measured at 2 K for the three samples. Data from mono-metallic Co particles of 1.5 nm diameter[10] are also included for comparison. All systems are found to be magnetic and display ferromagnetic behaviour with hysteresis. As a general tendency, on increasing the Rh concentration, the coercive field increases as well as the irreversible field up to and above 5 T. The differential high field susceptibility also increases, and none of the magnetization curves are saturated in this range of field. At 5 T, the magnetization per Co atom first increases and then decreases with increasing Rh concentration.

At higher temperature, the hysteresis disappears and the magnetization progressively decreases. This behaviour corresponds to the transition from a ferromagnetic behaviour to a super-paramagnetic one. This transition is confirmed by the behaviour of the susceptibility. The zero-field cooled and field-cooled susceptibility curves (measured at 1 mT) display the same typical shape (see Fig. 2 of ref. 6). The magnetization displays a narrow maximum which temperature corresponds to the blocking temperature, *i.e.* the transition from the superparamagnetic to the blocked ferromagnetic state. The same behaviour is observed for all the samples with

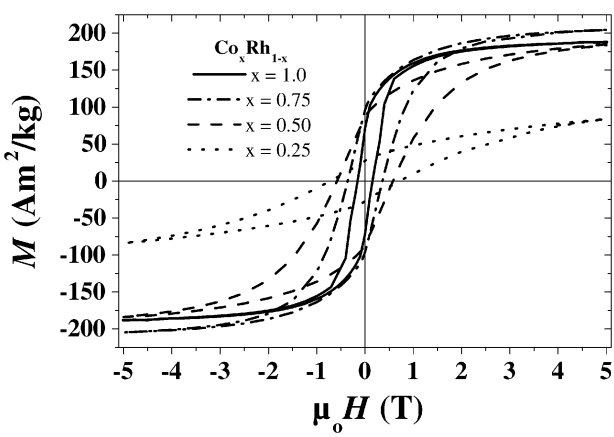

Fig. 1 Hysteresis loops measured at 2 K for bimetallic Co_xRh_{1-x} nanoparticles (diameter $\phi \simeq 2$ nm) for different Co concentrations x.

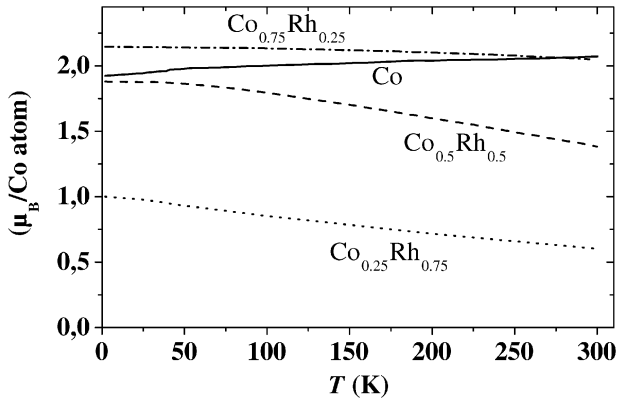

Fig. 2 Temperature dependence of the mean magnetic moment per Co atom in bimetallic Co_xRh_{1-x} nanoparticles ($\phi \simeq 2$ nm) for different Co concentrations x.

different blocking temperatures as a consequence of the different size distributions and effective anisotropy. We use the formalism described in ref. 6 and 10 to determine the size distributions, the variation of the spontaneous magnetization *versus* temperature $M_S(T)$ and the effective anisotropy K_{eff}.

The results plotted in Fig. 2 demonstrate that alloying with Rh induces a stronger dependence of M_S *vs.* temperature. The plot of the spontaneous magnetization with temperature can be fitted with a Bloch type law, the slope decreases while the Rh ratio increases. A surprisingly small increase of $M_S(T)$ is observed for pure Co as is also observed for free clusters by Billas *et al.*[11]

These data demonstrate that the Rh atoms in the $Co_{0.5}Rh_{0.5}$ clusters have a strong induced magnetic moment. The L_2 and L_3 XMCD signals are of the same order of magnitude, with opposite signs, indicating that the orbital contribution (L_z) is small compared to the spin one (S_z). Using Thole and Carra's sum rules,[12] we estimate the ratio $L_z/S_z = 0.066$.

The main experimental results can be summarized as follows: (i) For all the studied chemical compositions the clusters are magnetic. (ii) The cluster structure is closed packed with a tendency to fcc-like structure at least for low x_{Co} (iii) The mean NN distance in the cluster is very close to that of bulk Rh. (iv) The magnetic moment per Co atom is significantly enhanced with respect to the corresponding bulk alloy of similar concentration. (iv) The Rh atoms carry non vanishing spin and orbital magnetic moments. Despite all these interesting findings a number of questions still deserve to be clarified. For example, how does the cluster structure and distribution of Co and Rh within the cluster affect the magnetic behaviour? Can one infer any trends on the most likely chemical arrangement from the magnetic behaviour? What can be said about the role of segregation *versus* intermixing at the CoRh interface? How important are the orbital magnetic moments for the interpretation of experiment? And, is it possible to account for the measured magnetic moments quantitatively? In the following section we intend to address these kinds of questions from the point of view of theory by performing self-consistent calculations on Co_NRh_M as a function of size, structure and composition.

3. Theory

For the theoretical investigations we consider a d-band Hamiltonian given by ref. 13 and 14

$$H = H_0 + H_C + H_{SO}. \quad (1)$$

The first term

$$H_0 = \sum_{im,jm'} t_{ij}^{mm'} \hat{c}_{im\sigma}^{\dagger} \hat{c}_{jm'\sigma} \tag{2}$$

takes into account inter-atomic hybridizations between the orbitals m and m' of atoms i and j. In the usual notation, $\hat{c}_{im\sigma}^{\dagger}$, $\hat{c}_{im\sigma}$, and $\hat{n}_{im\sigma} = \hat{c}_{im\sigma}^{\dagger}\hat{c}_{im\sigma}$ refers to the creation, annihilation, and number operator for a spin-σ electron at orbital im. The Coulomb interaction term H_C is treated in the unrestricted Hartree–Fock approximation and may be written as

$$H_C = \sum_{im\sigma} \Delta\varepsilon_{im\sigma}\, \hat{n}_{im\sigma}, \tag{3}$$

where

$$\Delta\varepsilon_{im\sigma} = \sum_{m'} \left[\left(U_{mm'} - \frac{J_{mm'}}{2} \right) \nu_{im'} - \frac{\sigma}{2} J_{mm'} \mu_{im'} \right] \tag{4}$$

are the orbital- and spin-dependent shifts of the d levels that depend on the local occupations $\nu_{im} = \langle \hat{n}_{im\uparrow} \rangle + \langle \hat{n}_{im\downarrow} \rangle$ and spin polarizations $\mu_{im} = \langle \hat{n}_{im\uparrow} \rangle - \langle \hat{n}_{im\downarrow} \rangle$. The direct and exchange Coulomb integrals $U_{mm'}$ and $J_{mm'}$ are expressed in terms of the three independent radial Coulomb integrals $F^{(0)}$, $F^{(2)}$, and $F^{(4)}$, whose values can be derived from the known atomic ratios.[15] In this way atomic symmetry is strictly respected and all Hund's rules are naturally fulfilled. The Coulomb interactions $U_{mm'}$ and $J_{mm'}$ that define the self-consistent equations [eqn (4)], may be treated in a simple way by the so-called orbital polarization (OP) approximation.[18,19,22] This approach has been proposed in the context of first principles studies of TMs in order to enhance phenomenologically the effects of Hund's rule orbital polarizations and to correct for the systematic underestimations of the orbital moments obtained with the usual exchange and correlation density functionals. In this way numerous important predictions of the orbital magnetic moments in bulk, surfaces and deposited atoms have been obtained.[19–21] Within the present model the OP term is given by $H_{OP} = -B\Sigma_i \hat{L}_{i\delta}{}^2$ where $B = (9F^{(0)} - 5F^{(4)})/441$ is the Racah coefficient. The corresponding mean-field energy levels are then written as[14]

$$\Delta\varepsilon_{im\sigma} = \left(U - \frac{J}{2} \right) \nu_i - \frac{\sigma}{2} J \mu_i - B \langle L_{i\delta} \rangle m. \tag{5}$$

Here, $U = \overline{U_{mm'}} = F^{(0)}$ and $J = \overline{J_{mm'}} = (F^{(2)} + F^{(4)})/14$. In this context the OP approximation is equivalent to assuming that the orbital dependence of the Coulomb integrals has the form $U_{mm'} - U = J_{mm'} - J = -Bmm'$, which is the same for direct and exchange interactions. In practice, the OP calculations are much simpler than the rigorous orbital dependent treatment. In fact, they are not much more demanding than the simplest orbital independent approach,[24] since they require a self-consistent determination of only ν_i, μ_l and $\langle L_{i\delta} \rangle$ at all atoms. For the large clusters we use this approximation since it has been shown to yield similar results as the more demanding calculation in which the full orbital dependence of the Coulomb integrals are considered.[14] Notice that if $B = 0$ we obtain the simplest mean field approximation for eqn (5).[23–26]

Finally, the third term

$$H_{SO} = -\xi \sum_{i,m\sigma,m'\sigma'} (\vec{\boldsymbol{L}}_i \cdot \vec{\boldsymbol{S}}_i)_{m\sigma,m'\sigma'}\, \hat{c}_{im\sigma}^{+}\, \hat{c}_{im'\sigma'} \tag{6}$$

takes into account spin–orbit interactions, where $(\vec{\boldsymbol{L}}_i \cdot \vec{\boldsymbol{S}}_i)_{m\sigma,m'\sigma'}$ refers to the intra-atomic matrix elements of $\vec{\boldsymbol{L}} \cdot \vec{\boldsymbol{S}}$. H_{SO} couples the up and down spin-manifolds and introduces the dependence of the magnetic properties on the relative orientation between the magnetization direction and the geometrical structure of the cluster.

The average local orbital moments $\langle L_{i\delta}\rangle$ at atom i are calculated from

$$\langle L_{i\delta}\rangle = \sum_{\sigma}\sum_{m=-2}^{2}\int_{-\infty}^{\varepsilon_F} m\rho_{im\sigma}^{\delta}(\varepsilon)\,\mathrm{d}\varepsilon, \tag{7}$$

where m indicates the magnetic quantum number. The quantization axis of the orbital momentum is thereby taken to be the same as the spin quantization axis.

The electronic energy per atom

$$E_{\delta} = \frac{1}{N}\sum_{i} E_{\delta}(i) \tag{8}$$

can be written as the sum of local contributions

$$E_{\delta}(i) = \sum_{m\sigma}\left[\int_{-\infty}^{\varepsilon_F} \varepsilon\rho_{im\sigma}^{\delta}(\varepsilon)\,\mathrm{d}\varepsilon - E_{im\sigma}^{\mathrm{dc}}\right] \tag{9}$$

corresponding to each atom i of the cluster. Here $E_{im\sigma}^{\mathrm{dc}} = (1/2)\Delta\varepsilon_{i\sigma}\,\langle\hat{n}_{im\sigma}\rangle$ stands for the double-counting correction. The MAE is defined as the change ΔE in the electronic energy E_{δ} associated to a change in the orientation of the magnetization. Thus, positive (negative) values of the anisotropy energy $\Delta E_{xz} = E_x - E_z$ indicate that the easy (hard) axis is along the z direction.

The parameters used in the calculations are then specified as follows. The two-center d-electron hopping integrals are given by the canonical expression in terms of the corresponding bulk d-band width. The intra-atomic Coulomb integrals $U_{mm'}$ and $J_{mm'}$ are expressed in terms of the three independent radial Coulomb integrals $F^{(0)}$, $F^{(2)}$, and $F^{(4)}$ allowed by atomic symmetry.[15] These are chosen by taking the ratios $F^{(0)}/F^{(2)}$ and $F^{(4)}/F^{(2)}$ from atomic calculations[27] and by fitting the value of $F^{(2)}$ to reproduce the bulk Co spin moment [$\overline{U_{mm'}} = F^{(0)} = 13.5$ eV and average exchange integral $\overline{J_{mm'}} = (F^{(2)} + F^{(4)})/14 = 0.74$ eV]. In the case of Rh we use $F^{(2)}$ such as $J_{\mathrm{av}}^{\mathrm{Rh}} = 0.48$ eV, which have been obtained from density functional calculations (Stoner theory) taking into account correlation effects beyond the local spin density approximation.[28] Notice that for properties like the spin and orbital magnetic moments, which derive directly from the spin-polarized density distribution, a size independent $U_{mm'}$ ($J_{mm'}$) has been proved to be a good approximation. Using these values for the radial integrals we estimate the Racah coefficient $B = (9F^{(2)} - 9F^{(4)})/441$ ($B_{\mathrm{Co}} = 0.08$ eV and $B_{\mathrm{Rh}} = 0.05$ eV). In this way, only one parameter [$F^{(2)}$] is involved in the determination of the Coulomb integrals. The SO coupling constants ξ(Co) = 0.088 eV and ξ(Rh) = 0.180 eV are taken from ref. 16. As suggested by experiment,[6,9] we consider fcc-like clusters formed by a central atom and its successive shells of NN's. For Co–Rh this corresponds to a $\mathrm{Co}_N(\mathrm{Rh}_M)$ core covered with a $\mathrm{Rh}_M(\mathrm{Co}_N)$ shell. The structural effects are discussed by considering additional geometries, namely octahedral-like fcc and polytetrahedral-like structures.

The local densities of electronic states (DOS) $\rho_{im\sigma}^{\delta}(\varepsilon)$ are determined self-consistently for each orientation δ of the spin magnetization $\vec{\boldsymbol{S}}$. In this paper we consider $\delta = z$, along a principal C_{n} symmetry axis of the cluster, and $\delta = x$ along a nearest neighbor (NN) bond perpendicular to z. In the case of low-symmetry structures a full vectorial calculations as a function of both, the polar angle θ (between the magnetization $\vec{\boldsymbol{M}}$ and the z axis) and the azimuthal angle ϕ were performed. The associated single-particle problem is solved by using Haydock–Heine–Kelly's recursion method.[17] The local orbital occupations ν_{im} and spin polarizations μ_{im} are determined with an accuracy $\varepsilon \backsimeq 10^{-10}$ electrons per atom or better, which allows to derive the MAEs reliably.

4. Discussion

The calculated spin and orbital magnetic moments for Co–Rh clusters are shown in Table 1. The results for a 43-atom fcc-like spherical cluster formed by a central atom and its successive shells of NN's correspond to a Co_{19} (Rh_{19}) core covered with a $Rh_{24}(Co_{24})$ shell. The direction of magnetization $\delta = z$ is along a principal C_n symmetry axis of the cluster, and $\delta = x$ along a nearest neighbor (NN) bond perpendicular to z. In the case of Co_{19} the easy direction xy is along the central atom

Table 1 Theoretical results for the magnetic properties of Co_NRh_M clusters: total magnetic moment per cluster atom $\bar{\mu}_T = \langle L_T \rangle + 2\langle S_T \rangle$, total magnetic moment per Co atom $\bar{\mu}_{N_{Co}}$, orbital magnetic moment per atom $\langle L_T \rangle$ along the easy axis δ, and orbital-to-spin moment ratio $\frac{\bar{L}}{2\langle S \rangle}$(Rh) at the Rh atoms. The results are shown as a function of Co composition $x_{Co} = \frac{N}{(N+M)}$. The magnetic moments are in Bohr magnetons. The structure of the clusters is indicated: disordered alloys are denoted by (m); no indication refers to core-shell systems

Cluster	x_{Co}	$\bar{\mu}_T$	$\bar{\mu}_{N_{Co}}$	$\langle L_T \rangle$	$\frac{\langle L \rangle}{2\langle S \rangle}$(Rh)	δ
$N + M = 43$						
Co_{43}	1.00	1.98	1.98	0.29		x
$Co_{19}Rh_{24}$	0.44	0.80	1.44	0.06	0.07	z
$Rh_{19}Co_{24}$	0.56	1.40	2.51	0.30	0.14	x
$N + M = 79$						
Co_{79}	1.00	1.88	1.88	0.19		z
$Rh_{19}Co_{60}$	0.76	1.65	2.17	0.26	0.09	z
$Rh_{37}Co_{42}(m)$	0.53	1.40	2.62	0.22	0.10	z
$Rh_{55}Co_{24}$	0.30	0.67	2.22	0.11	0.08	z
$N + M = 87$						
			Spherical fcc			
Co_{87}	1.00	1.92	1.92	0.23		x
$Rh_{19}Co_{68}$	0.78	1.76	2.25	0.35	0.08	x
$Rh_{43}Co_{44}(m)$	0.51	1.29	2.56	0.26	0.08	z
$Rh_{67}Co_{20}(m)$	0.23	0.86	3.75	0.18	0.12	z
$N + M = 85$						
			Spherical fcc			
Co_{85}	1.00	1.89	1.89	0.20		xy
$Rh_{19}Co_{66}$	0.77	1.71	2.20	0.30	0.10	xy
$Rh_{43}Co_{42}(m)$	0.49	1.44	2.91	0.24	0.13	xy
$Rh_{61}Co_{24}$	0.28	0.62	2.20	0.11	0.17	z
$N + M = 70$						
			Polytetrahedral			
Co_{70}	1.00	2.00	2.00	0.31		x
$Rh_{17}Co_{53}$	0.76	1.84	2.43	0.47	0.03	x
$Rh_{38}Co_{32}$	0.46	1.28	2.80	0.35	0.20	z
$Rh_{52}Co_{18}$	0.26	0.85	3.30	0.25	0.14	z
$N + M = 72$						
			Polytetrahedral			
Co_{72}	1.00	2.07	2.07	0.41		x
$Rh_{22}Co_{50}$	0.69	1.91	2.76	0.60	0.11	x
$Rh_{40}Co_{32}$	0.44	1.64	3.70	0.52	0.21	x
$Rh_{52}Co_{20}$	0.28	1.31	4.73	0.47	0.23	x
$N + M = 405$						
			Spherical fcc			
Co_{405}	1.00	1.87	1.87	0.18		z
$Rh_{127}Co_{278}(m)$	0.68	1.36	1.98	0.19	0.02	z
$Rh_{199}Co_{206}(m)$	0.51	1.05	2.07	0.16	0.06	z
$Rh_{201}Co_{204}$	0.50	1.04	2.05	0.16	0.01	z

and one of the vertices in the plane x–y. The direction δ yielding the lowest-energy is indicated. For comparison, results for Co_{43} are also given. First one observes that the total magnetic moment per atom $\bar{\mu}_T$ decreases with Co concentration x_{Co} ($\bar{\mu}_T$ = 1.98 μ_B for x_{Co} = 1.00 and $\bar{\mu}_T$ = 0.80 μ_B for x_{Co} = 0.44 with a Co_{19} core and $\bar{\mu}_T$ = 1.40 μ_B for x_{Co} = 0.56 with a Rh_{19} core). Notice the large reduction of $\bar{\mu}_T$ if a Co_{19} core is assumed. In contrast, the cluster having a Rh_{19} core still has a significant $\bar{\mu}_T$. This is mainly due to two effects: the larger NN bond-length in the Rh_{19} core and to the orbital contribution ($\langle L_T \rangle$ = 0.30 μ_B) of the Co surface atoms in $Rh_{19}Co_{24}$. Still, even in this case, $\bar{\mu}_T$ is smaller for x_{Co} = 0.56 than for x_{Co} = 1.00. This trend changes if the average magnetic moment per Co atom $\bar{\mu}_{N_{Co}}$ in Co–Rh clusters having a Rh core is considered instead of $\bar{\mu}_T$. In this case, $\bar{\mu}_{N_{Co}}$ increases with decreasing x_{Co} ($\bar{\mu}_{N_{Co}}$ = 1.98 μ_B for x_{Co} = 1.00 and $\bar{\mu}_{N_{co}}$ = 2.51 μ_B for x_{Co} = 0.56), indicating that the Rh contribution to the total moment is significant [μ_{NCo}(Rh) $\simeq$ 0.50 μ_B]. The fact that the Co–Rh clusters are more likely to have a Rh core seems to be in agreement with the experimental findings of the NN's bond-length and magnetic moment per Co–Rh unit.[6] (In fact the experiments show that the NN's bond-length of the cluster is very similar to that of bulk Rh and that $\bar{\mu}_{N_{co}} \simeq 2.38\ \mu_B$).[6] Furthermore, due to the induced magnetic moment in Rh atoms, the ratio $\frac{\langle L \rangle}{2\langle S \rangle}$(Rh) = 0.14 is significant. As will be discussed later, the calculated $\frac{\langle L \rangle}{2\langle S \rangle}$(Rh) for clusters with size of about 400 atoms is smaller. At this stage, one concludes that Co–Rh clusters with a Rh core have a significant induced moment at Rh atoms.

Results for $N + M$ = 70, 72, 79, 85 and 87 are shown in Table 1 in order to infer the effect of structure and Co composition on the magnetic properties. Three cases are analyzed: spherical fcc, octahedral fcc and polytetrahedral structures. An illustration of the considered structures is presented in Fig. 3. In the case of octahedral structures full vectorial calculations as a function of both, the polar angle θ between the magnetization $\vec{M}$ and the z axis and the azimuthal angle ϕ were performed. First, we compare the results of the spherical clusters with $N + M$ = 79 and $N + M$ = 87 [See Fig. 3(a) and (b)]. Notice that the 87-atom cluster is made up by taking the 79-atom cluster with an additional shell of 8 atoms. The results show that magnetic moments μ_T and $\mu_{N_{Co}}$ follow the same trends as those found in the smaller clusters, i.e., μ_T ($\mu_{N_{Co}}$) decreases (increases) with decreasing x_{Co} concentration and that the values of $\frac{\langle L \rangle}{2\langle S \rangle}$(Rh) = 0.09 − 0.12 μ_B are similar. One also observes that the average magnetic moments are larger in the 87-atom cluster than in the 79-atom cluster. This is mainly due to the larger orbital moment contribution of the low-coordinated Co surface atoms [the outermost 8 atoms in Fig. 3(b)]. Similar results are also found for the 85-atom cluster with octahedral structure. However, the results for $x_{Co} \simeq 0.5$ deserve special attention. Let us first notice that in this cluster there are 66 surface atoms. Thus, in order to have $x_{Co} \simeq 0.5$ and keeping a Rh core (with 19 atoms), 24 Rh atoms should be at the surface. The induced magnetic moments at the Rh atoms are larger since they have only low coordinated Co atoms as NNs. As a consequence, μ_T and $\mu_{N_{Co}}$ increase. Therefore, Co–Rh clusters having segregated Co atoms result in smaller average magnetic moments than in the case of mixed clusters.

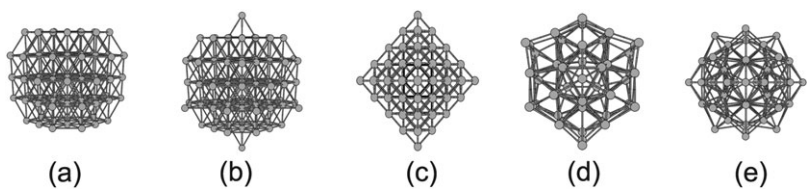

Fig. 3 Illustration of the cluster geometries considered in the calculations: (a) spherical fcc ($N + M$ = 79), (b) spherical fcc ($N + M$ = 87), (c) octahedral fcc ($N + M$ = 85), (d) polytetrahedral ($N + M$ = 70), and (e) polytetrahedral ($N + M$ = 72).

Larger values of μ_T and $\mu_{N_{Co}}$ are expected if the symmetry is further reduced. In fact, it has been argued that the structure of Co–Rh clusters is polytetrahedral for large Co concentration.[9] Two types of polytetrahedral growth were considered in this case: the structure of the 70-atom (72-atom) cluster is made up by growing slightly strained face-sharing tetrahedra over a hexahedron (13-atom icosahedron) [see Fig. 3(d) and (e)]. Notice the larger values of μ_T and $\mu_{N_{Co}}$ as compared with those of clusters of similar sizes (see, Table 1 for $x_{Co} \simeq 0.75$). This is due to the large contribution of the Co orbital moments at the surface [*i.e.*, for the 72-atom cluster, $\langle L \rangle$(Co) $\simeq$ 1.0 μ_B at the surface].

The results for large fcc spherical clusters having 405 atoms are also shown in Table 1. Notice that μ_T and $\mu_{N_{Co}}$ follow the same trends as a function of x_{Co} as in the previous studied clusters. However, the value of $\frac{\langle L \rangle}{2\langle S \rangle}$(Rh) $\simeq$ 0.06 is smaller than the one obtained in smaller sizes.

The environment dependence of the local orbital moments $\langle L_\delta \rangle(j)$ provides further insight into the magnetic behaviour. Fig. 4 displays $\langle L_\delta \rangle(j)$ in the considered fcc-like clusters, where $j = 1$ refers to the central atom and $j > 1$ to the successive NN shells. The sites corresponding to the Co(Rh) atoms are indicated. One observes that $\langle L_\delta \rangle(j)$ generally increases with j, showing some oscillations as we move from the center to the surface of the cluster. Notice the particularly large values of $2\langle S_\delta \rangle + \langle L_\delta \rangle$ which corresponds to the Rh atoms at $j = 12$ and $j = 14$. It is important to note that the Rh contributions to the total magnetic moment μ_T amount to about 20% [μ_{Rh} =

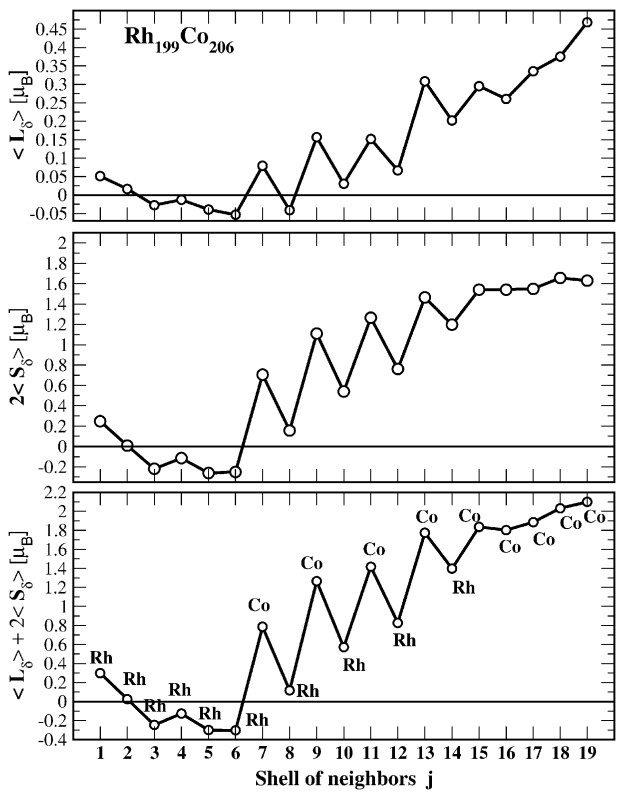

Fig. 4 Local orbital $\langle L(i) \rangle$, spin $2\langle S(i) \rangle$ and total $2\langle S(i) \rangle + \langle L(i) \rangle$ magnetic moment along the easy axis of a 405-atom fcc-like Co_xRh_{1-x} cluster with $x \simeq 0.5$. The results correspond to the average at each NN shell j surrounding the central atom $j = 1$. The shells correspond to a Rh core surrounded by successive Rh and Co shells (as indicated in the figure). The straight lines connecting the points are a guide to the eye.

Table 2 Shell average of the magnetic anisotropy energy $\Delta E_{zx}(j) = E_x(j) - E_z(j)$ of an fcc-like Co_NRh_M clusters having $N + M = 55$ atoms. The results refer to each NN shell j surrounding the central atom $j = 1$. $\Delta E_{zx} = E_x - E_z$ stands for the cluster average MAE. The direction z is taken along a C_n principal symmetry axis of the cluster and x along a NN bond perpendicular to z. The direction δ yielding the lowest-energy is indicated

	Shell j						
Cluster	1	2	3	4	5	ΔE_{xz}	δ
Co_{55}	1.00	−0.22	1.38	−1.33		−0.17	xy
$Co_{43}Rh_{12}$	1.00	0.02	0.35	0.35	−1.15	−0.43	x
$Rh_{13}Co_{42}$	0.44	−0.04	0.15	1.72	−1.70	0.13	z
$Rh_{43}Co_{12}$	0.56	−0.14	0.58	−0.12	−0.85	−0.53	x

$\langle L_\delta \rangle_{Rh} + 2\langle S_\delta \rangle_{Rh} = (0.2–0.5)\mu_B$]. The orbital and spin moments at the interfaces are mainly responsible for this increase of μ_{Rh}. These results demonstrate that it is the interface, rather than just the reduction of local coordination number, which is

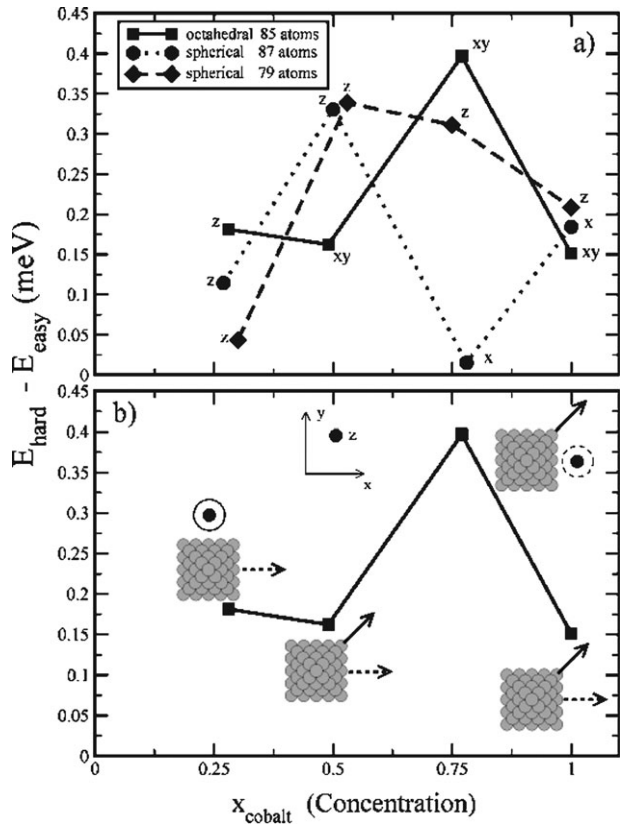

Fig. 5 (a) Magnetic anisotropy energy ΔE of Co_MRh_N clusters having $N + M = 79$, 85 and 87 atoms as a function of Co concentration. The corresponding structures are illustrated in Fig. 4. The labels x, xy, and z indicate the easy magnetization axis, where z refers to the direction along a principal C_n symmetry axis, x is along a NN bond perpendicular to z, and xy refers to the diagonal between the x and y axes [see the inset of figure (b)]. (b) Illustration of the easy axis (solid arrows for x and xy or solid circle for z) and hard axis (dashed arrows or dashed circle) of the 85-atom octahedral fcc cluster, as obtained from full vectorial calculations. A top view of the cluster structure is shown taken from the z principal C_4 symmetry axis. The directions of the magnetization x, y and z are illustrated in the inset.

responsible for the enhancement of magnetic moments. The calculated values well match the experimental ones, when considering both the spin and orbital contributions of the magnetic moments. It should be noticed that these calculations nicely reproduce the evolution of the magnetism with the Rh concentration and allow us to conclude that segregated nanoparticles containing a Rh core and a Co shell with some intermixing at the interface is the most likely scenario.

The interactions between magnetic ad-atoms and metallic substrates often lead to redistributions of the spin-polarized density and to changes in the electronic structure which affect sensitively the spin–orbit energies. The results shown in Table 2 indicate that the interface of Co–Rh plays the main role in determining the stable magnetization direction of the system. In fact, a rich and complex environment dependence of ΔE_{xz} is obtained by manipulating the interface. Replacing the Co core (Rh shell) by a Rh core (Co shell) changes the easy axis (see Table 2). Once again, the contribution of the local ΔE_{xz} to the MAE stabilizes the direction of magnetization. The environment dependence of ΔE_{xz} can be viewed as the result of two main contributions: the changes in the electronic structure of the Co cluster due to Co–Rh hybridizations and the local MAE of the interface Rh atoms which carry small magnetic moments.

Additional interesting magneto-anisotropic behaviour is expected if mixing of the 3d and 4d elements at the interface is allowed. Let us discuss in more detail the results for the MAE in larger clusters. A remarkable behaviour of the MAE as a function of x_{Co} is observed in Fig. 5. The results show that the MAE increases or decreases about 100% if the Co concentration changes from $x_{Co} = 1.00$ $x_{Co} = 0.75$ [see Fig. 5(a)]. Moreover, notice that the particular structure of the octahedral fcc cluster results in a large in-plane magnetic anisotropy energy (even larger than the usual off-plane MAE). In Fig. 5(b) results are shown for the MAE as a function of x_{Co}. Notice that only for $x_{Co} = 0.25$ the easy axis corresponds to the z direction. This shows the importance of performing full vectorial MAE calculations for structures having no spherical symmetry. A direct comparison of these results cannot be performed for several reasons, the main one being the strong dependence of the MAE with respect to the size, chemical order and structure. The effective anisotropy measured for the nanoparticles is in the range of 0.05–0.07 meV at^{-1}. It corresponds to the case of the less anisotropic clusters. Calculations for bigger nanoparticles are in progress.

5. Conclusion

In conclusion, it has been shown that alloying a 3d transition metal with a 4d element offers the possibility of tailoring new magnetic materials with optimized magneto-anisotropic properties for specific technological purposes. The magnetic moments of Co_xRh_{1-x} were determined using both experimental and theoretical approaches. The present discussion should encourage the development of new experimental work as well as further theoretical improvements. For example, it would be worthwhile to investigate more systematically the dependence of the magnetic properties on the geometry of the cluster and its immediate environment. This is relevant for the comparison between theory and experiment, since the morphology of the nanoparticles can be tuned, at least to some extent, by changing the growth and deposition conditions or by subsequent annealing. The well-known sensitivity of TM magnetism to the specific local atomic environments lets us expect a wide variety of interesting behaviours. From a theoretical perspective, it would be interesting to introduce a larger flexibility in the self-consistent calculations by allowing for non-collinear spin polarizations, since the SO interactions break the conservation of S_z, and since it has been shown that the magnetization direction giving the lowest local energy $E_\delta(i)$ is often different for different atoms i.[29]

References

1 See, for instance, *Nanoscale Materials*, ed. Prashant V. Kamat and Luis M. Liz Marzan, Kluwer Academic Press, Boston, USA, 2003.
2 J. Bansmann, S. H. Baker, C. Binns, J. A. Blackman, J.-P. Bucher, J. Dorantes-Dávila, V. Dupuis, L. Favre, D. Kechrakos, A. Kleibert, K.-H. Meiwes-Broer, G. M. Pastor, A. Perez, O. Toulemonde, K. N. Trohidou, J. Tuaillon and Y. Xie, *Surf. Sci. Rep*., 2005, **56**, 189.
3 (*a*) A. J. Cox, J. G. Louderback and L. A. Bloomfield, *Phys. Rev. Lett*., 1993, **71**, 923; (*b*) A. J. Cox, J. G. Louderback, S. E. Apsel and L. A. Bloomfield, *Phys. Rev. B*, 1994, **49**, 12295.
4 B. V. Reddy, S. N. Khanna and B. I. Dunlap, *Phys. Rev. Lett*., 1993, **70**, 3323.
5 P. Villaseñor González, J. Dorantes-Dávila, G. M. Pastor and H. Dreyssé, *Phys. Rev. B*, 1997, **55**, 15084.
6 D. Zitoun, M. Respaud, M.-C. Fromen, M. J. Casanove, P. Lecante, C. Amiens and B. Chaudret, *Phys. Rev. Lett*., 2002, **89**, 037203.
7 (*a*) S. Dennler, J. Morillo and G. M. Pastor, *J. Phys.: Condens. Matter*, 2004, **16**, S2263; (*b*) S. Dennler, J. Morillo and G. M. Pastor, *Surf. Sci*., 2003, **532–535**, 334.
8 D. Zitoun, C. Amiens, B. Chaudret, M. Respaud, M.-C. Fromen, P. Lecante and M. J. Casanove, *New J. Phys*., 2002, **4**, 77.1–77.11.
9 F. Dassenoy, M. J. Casanove, P. Lecante, M. Verelst, T. Ould Ely, C. Amiens and B. Chaudret, *J. Chem. Phys*., 2000, **112**, 8137.
10 M. Respaud, J. M. Broto, H. Rakoto, A. R. Fert, L. Thomas, B. Barbara, M. Verelst, E. Snoeck, P. Lecante, A. Mosset, J. Osuna, T. Ould Ely, C. Amiens and B. Chaudret, *Phys. Rev. B*, 1998, **57**, 2925.
11 I. M. L. Billas, A. Châtelain and Walt A. de Heer, *Science*, 1994, **265**, 1682.
12 (*a*) B. T. Thole, Paolo Carra, F. Sette and G. van der Laan, *Phys. Rev. Lett*., 1992, **68**, 1943; (*b*) Paolo Carra, B. T. Thole, Massimo Altarelli and Xindong Wang, *Phys. Rev. Lett*., 1993, **70**, 694.
13 R. Guirado-López, J. Dorantes-Dávila and G. M. Pastor, *Phys. Rev. Lett*., 2003, **90**, 226402.
14 G. Nicolas, J. Dorantes-Dávila and G. M. Pastor, *Phys. Rev. B*, 2006, **74**, 014415.
15 J. C. Slater, *Quantum Theory of Atomic Structure*, McGraw-Hill Book Co. Inc., New York, vol. I and II, 1960.
16 P. Bruno, *Magnetismus von Festkörpern und Grenzflächen*, 1993 Ferienkurse des Forschungszentrums Jülich (KFA Jülich), ch. 24 and references therein.
17 R. Haydock, in *Solid State Physics*, edited by H. Ehrenreich, F. Seitz and D. Turnbull, Academic, New York, 1980, vol. 35, p. 215.
18 M. Brooks, *Physica B*, 1985, **130**, 6.
19 O. Hjortstam, J. Trygg, J. M. Wills, B. Johansson and O. Ericksson, *Phys. Rev. Lett*., 1996, **65**, 492.
20 (*a*) Olle Ericksson, Börje Johansson, R. C. Albers, A. M. Boring and M. S. S. Brooks, *Phys. Rev. B*, 1990, **42**, 2707; (*b*) Per Söderlind, Olle Ericksson, Börje Johansson, R. C. Albers and A. M. Boring, *Phys. Rev. B*, 1992, **45**, 12911.
21 P. Gambardella, S. Rusponi, M. Veronese, S. S. Dhesi, C. Grazioli, A. Dallmeyer, I. Cabria, R. Zeller, P. H. Dederichs, K. Kern, C. Carbone and H. Brune, *Science*, 2003, **300**, 1130.
22 I. V. Solovyev, A. I. Liechtenstein and K. Terakura, *Phys. Rev. Lett*., 1998, **80**, 5758.
23 (*a*) G. M. Pastor, J. Dorantes-Dávila and K. H. Bennemann, *Physica B*, 1988, **149**, 22; (*b*) G. M. Pastor, J. Dorantes-Dávila and K. H. Bennemann, *Phys. Rev. B*, 1989, **40**, 7642; (*c*) J. Dorantes-Dávila, H. Dreyssé and G. M. Pastor, *Phys. Rev. B*, 1992, **46**, 10432.
24 G. M. Pastor, J. Dorantes-Dávila, S. Pick and H. Dreyssé, *Phys. Rev. Lett*., 1995, **75**, 326.
25 J. Dorantes-Dávila and G. M. Pastor, *Phys. Rev. Lett*., 1996, **77**, 4450.
26 J. Dorantes-Dávila and G. M. Pastor, *Phys. Rev. Lett*., 1998, **81**, 208.
27 J. B. Mann, *Atomic Structure Calculations*, 1967, Los Alamos Sci. Lab. Rep. LA-3690.
28 (*a*) N. E. Christensen, O. Gunnarsson, O. Jepsen and O. K. Andersen, *J. Phys. (Paris)*, 1988, **49**, C8–17; (*b*) O. K. Andersen, O. Jepsen and D. Glötzel, *Highlights of Condensed Matter Theory*, ed. F. Bassani, F. Fumi and M. P. Tosi, North Holland, Amsterdam, 1985, p. 59.
29 (*a*) R. Félix-Medina, J. Dorantes-Dávila and G. M. Pastor, *Phys. Rev. B*, 2003, **67**, 094430; (*b*) R. Félix-Medina, J. Dorantes-Dávila and G. M. Pastor, *New J. Phys*., 2002, **4**, 1.1–1.14.

